Radar observation of extreme vertical drafts in the polar summer mesosphere

J. L. Chau[1], R. Marino[2], F. Feraco[2,3], J. M. Urco[1,4], G. Baumgarten[1], F.-J. Lübken[1], W. K. Hocking[5], C. Schult[1], T. Renkwitz[1], R. Latteck[1]

[1]Leibniz-Institute of Atmospheric Physics at the University of Rostock, Kühlungsborn, Germany
[2]Laboratoire de Mécanique des Fluides et d'Acoustique, CNRS, École Centrale de Lyon, Université Claude Bernard Lyon 1, INSA de Lyon, Écully, France
[3]Dipartimento di Fisica, Universitá della Calabria - Arcavacata di Rende (CS), Italy
[4]Department of Electrical and Computer Engineering and Coordinated Science Laboratory, University of Illinois Urbana-Champaign, Urbana, IL, USA
[5]Department of Physics and Astronomy, University of Western Ontario, London, Ontario, Canada

Key Points:

- First observations of extreme vertical velocities in the polar summer mesosphere.
- The observed solitary wave in a varicose mode resembles a mesospheric bore, with large vertical extent and vertical velocities.
- Such extreme events might have been missed or ignored in previous observations of vertical velocities or other mesospheric observations.

Corresponding author: Jorge L. Chau, chau@iap-kborn.de

Abstract

The polar summer mesosphere is the Earth's coldest region, allowing the formation of mesospheric ice clouds. These ice clouds produce strong polar mesospheric summer echoes (PMSE) that are used as tracers of mesospheric dynamics. Here we report the first observations of extreme vertical drafts (± 50 ms^{-1}) in the mesosphere obtained from PMSE, characterized by velocities more than five standard deviations larger than the observed vertical wind variability. Using aperture synthesis radar imaging, the observed PMSE morphology resembles a solitary wave in a varicose mode, narrow along propagation (3–4 km) and elongated (> 10 km) transverse to propagation direction, with a relatively large vertical extent ($\sim$13 km). These spatial features are similar to previously observed mesospheric bores, but we observe only one crest with much larger vertical extent and higher vertical velocities.

Plain Language Summary

Extreme events are ubiquitous of geophysical flows. Example of these events are tornadoes and Rogue waves in the lower atmosphere and oceans, respectively. In the mesosphere, the boundary of Earth's atmosphere and outer space, extreme events could also occur, although this region is poorly observed. Here we present the first observations of vertical velocities more than five times their expected standard deviation. These observations are possible by tracking and imaging strong mesospheric radar echoes that occur in the summer at polar latitudes, with a radar used in a radio camera mode. The morphology of our observations resembles previously observed instabilities called bores or wave walls, but with much larger vertical velocities and vertical extents.

1 Introduction

Extreme events are ubiquitous to geophysical flows, e.g., tornadoes or rogue waves (e.g., Tippett & Cohen, 2016; Adcock & Taylor, 2014). In the mesosphere (60–90 km), extreme events could also exist. This region is difficult to observe since it is too high for meteorological balloons, and too low for satellites to fly in and make in-situ measurements. Therefore, observations of extreme events and their respective impacts in this region are not easy to identify and study. Nonetheless, this atmospheric region hosts a number of interesting optical and radio phenomena like noctilucent clouds (NLC) and polar mesospheric summer echoes (PMSE) (e.g., Thomas & Olivero, 1986; Ecklund & Balsley, 1981; Hoppe et al., 1988).

During summer months at mid and high latitudes, the mesosphere is the coldest place on Earth with temperatures as low as 130 K due to dynamical processes that drive the atmosphere away from radiatively controlled state (e.g., Lübken et al., 1999). One of the most challenging, important, and intriguing mesospheric measurements are vertical winds. Vertical winds are usually smaller than horizontal winds, but they have significant effects on the atmospheric dynamics, composition, and electrodynamics (e.g., Larsen & Meriwether, 2012). Their mean synoptic-scale values are expected to be in the order of centimeters per second and are difficult to measure directly (e.g., Gudadze et al., 2019). On the other hand measurements made with ground-based radars, passive optics, lidars, as well as in-situ chemical traces, show high values varying by up to ± 10 ms^{-1} (e.g., Hoppe & Fritts, 1995; Gardner & Liu, 2007; Lehmacher et al., 2011). Similar and even higher values have been observed at higher altitudes in the thermosphere (e.g., Larsen & Meriwether, 2012). These high values can occur with the same sign for minutes to hours.

Although part of this variability is attributed to Kelvin-Helmholtz, mesospheric bores and other instabilities (e.g., Chau et al., 2020), the drivers for the majority of observations of large and/or persistent values are not obvious. Waves propagating through the region appear to be connected to the vertical wind variability; either they come from below or are generated locally via instabilities, nonlinear interaction with other waves or turbulence (e.g., Gardner et al., 1995; Fritts et al., 2004; Larsen & Meriwether, 2012). Moreover, high variability in vertical winds have been reproduced in direct numerical simulations (DNS) in flows similar to those in the mesosphere (Marino et al., 2015), including extreme values under some special flow conditions (Feraco et al., 2018). Understand-

ing and characterizing the vertical wind variability of the mesosphere and higher altitudes (thermosphere) are important for explaining their effects on dynamics, composition, chemistry, and electrodynamics of these regions (e.g., Larsen & Meriwether, 2012).

In this work, we focus on extreme vertical drafts observed in the polar summer mesosphere. These observations have been made with the Middle Atmosphere Alomar Radar System (MAARSY) located in northern Norway (69.30°N, 16.04°E). Observations of PMSE have been routinely made with MAARSY since 2010 (Latteck et al., 2012). After more than 20 years of active research, the physics behind PMSE is well understood. Their signal strength depends on electron density, turbulence, and charged-ice particles (e.g., Rapp & Lübken, 2004) and they are good tracers of atmospheric winds (e.g., Sato et al., 2017).

Based on two summers of continuous observations and many years of experience, the event we present is extreme since our measured vertical velocities reach values as high as more than five times their standard deviation (σ_w). We start describing the observing modes. Our radar results are presented in Section 3, followed by a discussion and possible connections to previously observed mesospheric instabilities.

2 Radar observing modes

MAARSY is an active phased array that consists of 433 three-element cross-polarized Yagi antennas and operates at 53.5 MHz. Its main beam one-way half-power beam-width is 4°. On reception, either all 433 elements, or up to 7 groups of 49 elements, or up to 15 out of 55 groups of 7 elements can be used (e.g., Latteck et al., 2012, for more details).

PMSE are routinely observed with MAARSY using two quasi-simultaneous main modes: (a) multi-beam, and (b) radar imaging (e.g., Gudadze et al., 2019; Urco et al., 2019). These modes have been used during the summers of 2016 and 2017, except for a few days where other modes were used to support special requests. Both modes run with 1 ms interpulse period. Since horizontal winds are expected to be within ± 150 ms^{-1}, the multi-beam mode has been configured to allow a Nyquist velocity of ± 35 ms^{-1}. On the other hand the radar imaging mode allows a Nyquist velocity of ± 175 ms^{-1}, suitable to study other echoes, e.g., non-specular meteor echoes (Chau et al., 2014).

Given the velocity aliasing in the multi-beam mode, in this work we use only data from the radar imaging mode, which observes for 30 s every 180 s. This mode uses only one vertically pointing transmitting beam using all 433 elements, while 16 antenna groups

are used on reception, 15 of them for radar imaging. A spectral moment method has been implemented to obtain: signal, mean radial velocity and spectral width. Radial velocities from slightly off-vertical locations could have contributions from horizontal velocities. However, unrealistic supersonic horizontal winds (more than 1500 ms^{-1}) would be required to generate the large ($\sim$ 50 ms^{-1}) observed velocities.

Radar imaging has been obtained by applying the Maximum Entropy method on the cross-spectra data from combinations of receiving antenna pairs (e.g., Hysell & Chau, 2006; Urco et al., 2019). Since the selected 15 receiving antennas do not have the same beam width, the imaging inversion has been performed only within $\pm 8^{\circ}$ zenith angles. This angular coverage also allows for the observation of PMSE outside the main illuminated area, if strong echoes are present there.

Besides the PMSE observations, in this work we also used the horizontal wind observations with a specular meteor radar (SMR) located also in Andoya (e.g., Chau et al., 2017). This system consists of one single element Yagi antenna on transmission and five single element antennas on reception arranged in an interferometer configuration. On reception echoes from meteor trails perpendicular to the line of sight are detected and identified. The radial velocity and location (range and angle) of each meteor trail within selected altitude and temporal bins are used to estimate a mean horizontal wind vector for that bin (e.g., Hocking et al., 2001). Such vector components are obtained assuming a homogeneous wind inside the illuminated area, i.e., a circle of approximately 400 km diameter at 86 km altitude.

3 Results

The extreme event of vertical drafts that occur on July 16, 2016 is shown in Figures 1a to 1c. Figure 1a shows the signal-to-noise ratio (SNR) as a function of altitude and time. The vertical velocities and spectral widths are shown in Figures 1b and 1c, respectively.

The event in question occurred between 04:25 and 05:00 universal time (UT) and is characterized by: (a) episodes of large vertical updrafts and downdrafts lasting a few minutes at around 86 km, (b) large spectral widths, and (c) echoes appearing to move up and down according to the measured mean vertical velocities, and (d) their strength increasing (decreasing) when going up (down). Outside this time interval, the PMSE spec-

tral moments behave within expected values, i.e., vertical velocities within ± 5 ms^{-1}, spectral widths below 5 ms^{-1}, and echoes occurring in multiple layers.

In Figures 1d to 1t normalized spectrograms for selected times around the extreme event are shown. Each spectrum is obtained from $\sim$30 s continuous observations. The striking features in this figure are the large positive and negative vertical drafts well outside $3\sigma_w$, reaching high absolute values (e.g., 65 ms^{-1} at 04:28:21 UT or -45 ms^{-1} at 04:36:03 UT). Except for the spectra at 04:41:11 (1o) and 04:43:46 (1n) UT, the spectra are composed of one or two velocity peaks at a given altitude. Given that the illuminated volume has a radius of about $\sim$ 5 km in the horizontal direction at these altitudes , the multi peak features are a result of multiple regions of enhanced backscattering within the illuminated volume. The presence of multiple peaks gives rise to large values of spectral widths. The red dashed lines indicate the $3\sigma_w$ based on two months of continuous observations in 2016.

From radar imaging, we have obtained spatial information of features within the illuminated volume. Figures 2a to 2f show selected 2D spatial planes of imaging around 04:30:54 UT. The large scale 30-min averaged horizontal winds obtained from a closely located specular meteor radar are shown in arrows as a reference. Radar imaging results clearly indicate that the extreme updrafts and downdrafts are localized in horizontal space, with 3–4 km width along the x axis, and at least 8–12 km elongation along the y axis, where x- and y-axis are rotated 50° East of North. An animation of similar frames from 04:00 to 05:30 UT every 150–170 s can be seen in Movie S1. The imaging results are also used to verify that the inferred vertical velocities are mainly due to vertical wind and not to a horizontal wind contamination, since areas of large vertical drafts are observed at or close to overhead inside the vertical transmitting beam. For typical mesospheric horizontal winds (± 150 ms^{-1}), their contamination in our vertical estimates would be at most within ± 4 ms^{-1}.

The temporal evolution of these spatial features is summarized in Figures 2g to 2n as function of x (i.e., X-Time Doppler-Intensity, XTDI) (left) and y (YTDI) (right) for selected altitudes. The extreme drafts are elongated along y at all altitudes, and drift along x. At 89 km, the updraft is observed to cover at least 16–20 km in x, appearing around 04:20 and disappearing around 04:45 UT. The irregularities causing these echoes move up from around 86 km and stay at 89 km for at least 25 min. At 81.5 km, down-

drafts are also elongated along the y axis and drift generally along x. However, they are only observed for 2–4 km along x and last less than 5 min. The latter suggests that the irregularities came down from 86 km or so and disappear after a few minutes. Later the echoes appear again around 04:55 due to irregularities coming from below and remain present at least until 05:30 UT. Both regions of updrafts and downdrafts drift at $\sim$11 ms^{-1} along x, North-East, with respect to an observer on the ground. Note that regions of large drafts are observed for a longer time in these plots than in the spectra plots in Figure 1, since the spectra were obtained using all 433 elements on transmission and reception. The duration, elongation and horizontal extent of the event should be taken as minimum values, given the relatively small observing volume, when compared to other imaging observations (e.g., airglow imagers).

Figure 3 shows profiles of horizontal wind magnitude and direction as well as their vertical gradients. These profiles were obtained with the SMR described above, around the time of the event. A moderate horizontal wind shear (24 ms^{-1}km^{-1}), occurs at the altitude where the extreme updrafts and downdrafts begin, i.e., 86 km. Recall that these are mean values representing an area of approximately 400 km diameter at 86 km obtained.

4 Discussion

The main features of the kilometer-scale extreme event presented here can be summarized as follows: (a) vertical drafts close to $5\sigma_w$ occur during a limited time of $\sim$30 minutes on July 16, 2016 around 0430 UT; (b) they occur between 80 and 90 km, (c) updrafts (downdrafts) up to 65 (45) ms^{-1} occur above (below) 86 km, are observed for long (short) time, and their associated echoes present larger (smaller) SNR than echoes at 86 km where they begin; (d) it is localized in horizontal space with widths of 3–4 km in the x axis, and elongated along the y axis; (e) at the center altitude, the vertical gradient of the background horizontal wind is the largest (24 ms^{-1}km^{-1}); (f) the PMSE layer thickness changes from 3 km (before the event) to 13 km (at the central time), (g) both drafts drift across the observing volume apparently against the mean horizontal wind at $\sim$11 ms^{-1}, therefore the duration, elongation and horizontal extent of the event should be taken as minimum values.

4.1 Verification of our observations

Since our reported vertical velocities are not expected and might be controversial, in this section we summarize briefly some of the actions we have performed to verify the validity of our vertical velocity estimates. The first obvious check was range aliasing. Our unambiguous range is 300 km, echoes coming from 380 km might be range aliased, however, their range, temporal, and spectral features do not correspond to such altitude. For example, if they were echoes from radar aurora, they would cover a much larger range (e.g., Chau & St.-Maurice, 2016). Moreover, plasma instabilities have been ruled out since: (a) the ionosphere was quiet for a few hours around the event, and (b) the altitude is too low for plasma instabilities to be generated (e.g., St.-Maurice & Chau, 2016). The former indicates that strong electric fields are not expected, while the latter is supported by high collision frequencies around 86 km.

Horizontal velocity contamination is a usual suspect on vertical velocity studies, particularly when studying their mean values (e.g., Gudadze et al., 2019). As we mentioned above without considering radar imaging, unrealistic huge supersonic horizontal velocities would be needed to explain the reported vertical velocities. Moreover in the imaging results, at a given altitude they would be shown with a transition from red to blue as the scattering center passes the beam center if the vertical velocity is very small. Figure 2g clearly shows that the upper/lower altitude regions are red/blue as the event transits the beam. At most we expect the horizontal contamination to be within ± 4 ms^{-1}.

The vertical velocity profile is not constant at all altitudes at the central time of the event (i.e., 04:30), instead, it shows a maximum upward value around 89 km, zero at 86 km, and maximum downward value around 82 km. A simple integration of this vertical profile, supports the observed vertical extension, i.e., a few kilometers in altitude in a few minutes.

4.2 Connection to mesospheric bores

A sketch based on the observations is shown in Figure 4. The SNR, vertical velocity, and spectral width from Figure 1 are combined into an altitude-time-Doppler intensity plot (e.g., Chau et al., 2020), with superimposed arrows indicating w directions, and expected regions of horizontal wind convergence (C) and divergence (D) (see below). Clearly, our observed event resembles a solitary wave oscillating in varicose mode, i.e., where the

upper part is rising, the lower part is falling, and viceversa. This varicose mode is expected in internal bores (e.g., Dewan & Picard, 2001) and has been directly observed in mesospheric bores (e.g., Fritts et al., 2020).

Our sketch together with the spatial features shown in Figure 2 resembles the mesospheric bore features of Bore 1 reported by Fritts et al. (2020), where they combined 2D images of PMC and lidar vertical profiling. As in the case of Fritts et al. (2020), we also expect that the observed vertical velocity divergence (convergence) ahead of (behind) the extreme event is accompanied by horizontal wind convergence (divergence). This horizontal wind behavior, unfortunately, could not be directly measured in our case. However, using vertical velocities from Figure 1i and assuming an incompressible flow, the estimated local horizontal wind convergence is $\sim$14 ms^{-1}km^{-1}, which is more than 100 times the measured mesoscale horizontal divergence in this region (Chau et al., 2017). Note that the large local horizontal wind convergence/divergence is expected at the central altitude and not where the high vertical velocities are observed.

The vertical dimensions of our event are more than two times larger than those reported by Fritts et al. (2020), i.e., $2h_1 \sim 13$ and $2h_0 \sim 3.0$ km, instead of 4.7 and 2.8 km, respectively, where $2h_1$ and $2h_0$ are the vertical extensions during the peak of the perturbation and before the perturbation. These dimensions imply a normalized bore amplitude $\beta = (h_1 - h_0)/h_0 \sim 3.33$ which is much larger than previously measured or inferred characteristics of mesospheric bores or wall waves (e.g., Taylor et al., 1995; Li et al., 2007; Smith et al., 2003, 2017). Vertical velocities in previous mesospheric bores have been expected or measured to be less than 10 ms^{-1} (e.g., Li et al., 2007).

Morphologically our extreme event resembles a mesospheric bore, but given its vertical dimensions, observed vertical velocities, and single observed crest, our event is unique. Unfortunately, temperature and density profiles are not available for this event. However, as in the case of typical mesospheric bores, we expect that our event is a consequence of an instability occurring in some type of ducting (Doppler, thermal or a combination of both). Ducting regions are ubiquitous, but mesospheric bores are not. Possible mechanisms that have been invoked to explain mesospheric bores might also explain our observations, e.g., interaction of gravity waves with the mean flow at a critical level (e.g., Dewan & Picard, 1998), non-linear internal gravity waves trapped within a thermal inversion layer (e.g., Seyler, 2005), etc. Interesting to note is that run 8 in Seyler (2005)

Table 1, reproduces a single-crest bore with larger amplitudes and Bore speeds than the other runs. However, none of the previous theories aimed to explain an event with the large β and very high vertical velocities that characterized our observations.

DNS results of stratified flows have predicted extreme vertical velocities localized in space and time under particular values of stratification, specifically with Froude number $\sim 0.1-0.01$ (Feraco et al., 2018). Although a one-to-one comparison with our event is difficult, the DNS results indicate that the resonant interaction between gravity waves and turbulent motions responsible for the simulated DNS results, might play a role in explaining our event. Such comparison with DNS results and possibly more events will be pursued on a future work.

4.3 How often mesospheric extreme events occur?

We have presented only one event showing extreme vertical velocities. At this point is difficult to infer if this is an isolated one-of-a-kind event, or if they occur more often but, due to their high velocities and spatio-temporal characteristics, have been ignored.

In the case of previous PMSE observations with MAARSY, the great majority were done with Nyquist velocities less than 30 ms^{-1}. Therefore, extreme drafts have been filtered out and cannot be recovered by their velocity values. In cases where larger Nyquist velocity have been used, they were presumably treated as outliers given their large values and relative short duration (e.g. Gudadze et al., 2019, Figure 4). In the latter cases, a careful reprocessing should be pursued to search for additional extreme drafts. Data obtained with small Nyquist might still be useful, if one looks for sudden vertical excursions (up and down).

Based on the possible relation to mesospheric bores that have been observed at different latitudes (Hozumi et al., 2019), such extreme drafts are not expected to be unique to the polar summer mesosphere. Thus, one should search for extreme vertical velocities at other latitudes, seasons, with a variety of instruments. For example, mesospheric solitary waves (solitons) reported from foil chaff experiments in the past, might have sampled a small spatial and temporal portion of an extreme event like the one reported here (Widdel, 1991).

Although our work is focused on vertical velocities, such extreme events should show up in other atmospheric variables, e.g., temperatures, airglow intensities, NLC brightness, etc. As far as we know, extreme events based on these parameters have not been reported so far, or they might have been ignored.

4.4 Potential impacts

In the particular case of the polar summer mesosphere, ice particles exist and they are the main reason for the presence of NLC and PMSE (e.g. Thomas & Olivero, 1986; Rapp & Lübken, 2004). Using expected temperature and pressure profiles from empirical models as well as the observed vertical drafts, we find that in our specific case the temperature increases significantly in the downdraft regions. This increase causes the reduction of ice particle radius in time scales of a few minutes (see Figure S1). In the case of PMSE, their volume reflectivity is mainly determined by the Schmidt number, which is proportional to the square of ice particle radius (e.g., Rapp & Lübken, 2004). Therefore a reduction of ice particle radius would mean a weaker PMSE. In Figure 1a, the strength of echoes decreases or echoes even disappear for the regions experiencing downdrafts. In the updraft regions, the strength of echoes increases but based on our calculations this increase is not related to the ice particle radius, instead it could be due to an increase of electron density. These simple calculations indicate that indeed ice particle radius is affected by extreme vertical drafts, and so are clouds and echoes relaying on it.

Like in the case of ice particles, other mesospheric species would also experience significant changes in altitude, and therefore their mixing ratios might change at a given altitude. The transport of photochemically inactive species across the turbopause by vertical winds enhances their concentration much more rapidly compared to turbulent mixing, which implies that extreme vertical updrafts are an effective mechanism to transport trace gases into the lower thermosphere. For example if Argon and molecular Nitrogen are brought to higher altitudes, e.g., from 90 to 110 km, it could take up to 3 h to fully mix these components, i.e., much longer than if these species would have stayed at 90 km (e.g., Von Zahn et al., 1990).

5 Conclusions

We report the first observations of extreme vertical drafts (± 50 ms^{-1}) in the mesosphere characterized by a solitary wave behavior in varicose mode. Although their horizontal and spatial structures resemble those of previously observed mesospheric bores, our event shows only one crest with a much larger vertical extent than previous observations. This vertical extension is consistent with the observed extreme vertical velocities.

Our current poor knowledge on these extreme drafts (formation, occurrence rate, duration, predictability) as well as limited observing capabilities in the mesosphere, should not impede the exploration of impacts on other fields where km-scale perturbations and instabilities and high vertical drafts might be important. As in the case of mesospheric bores, if they occur frequently a better understanding and characterization would contribute to the roles of such dynamics (including small-scale gravity waves and instability dynamics) in a number of parameters requiring parameterization in large-scale general circulation weather and climate models (e.g., Fritts et al., 2014, 2020). Further observations as well as theory and modelling efforts are still needed to find and identify the specific sources of mesospheric bores and our reported event.

Acknowledgments

This work was partially supported by the Deutsche Forschungsgemeinschaft (German Research Foundation) under project LU1174/8-1 (PACOG) of the research unit FOR1898, and under SPP 1788 (CoSIP) project CH1482/3-1 (CS-PMSE-MIMO). The authors would like to thank Nikoloz Gudadze for suggesting us to look at the PMSE observations from July 16, 2016.

Open Research Data Statement

PMSE radar spectra and imaging data as well as meteor wind data, can be found here `https://www.radar-service.eu/radar/en/dataset/RDOybenOQktKPLsT?token=MIPFqNPRJYOxNGsasNXi`.

References

Adcock, T. A. A., & Taylor, P. H. (2014). The physics of anomalous ('rogue') ocean waves. *Reports on Progress in Physics*, *77*(10). doi: 10.1088/0034-4885/77/10/

105901.

Chau, J. L., & St.-Maurice, J.-P. (2016). Unusual 5 m E region field-aligned irregularities observed from Northern Germany during the magnetic storm of 17 March 2015. *Journal of Geophysical Research: Space Physics*, *121*(10), 310–316. Retrieved from `https://agupubs.onlinelibrary.wiley.com/doi/abs/10.1002/2016JA023104` doi: 10.1002/2016JA023104

Chau, J. L., Stober, G., Hall, C. M., Tsutsumi, M., Laskar, F. I., & Hoffmann, P. (2017). Polar mesospheric horizontal divergence and relative vorticity measurements using multiple specular meteor radars. *Radio Science*, *52*(7), 811–828. doi: 10.1002/2016RS006225.

Chau, J. L., Strelnikova, I., Schult, C., Oppenheim, M. M., Kelley, M. C., Stober, G., & Singer, W. (2014). Nonspecular meteor trails from non-field-aligned irregularities: Can they be explained by presence of charged meteor dust? *Geophysical Research Letters*, *41*(10), 3336–3343. doi: 10.1002/2014GL059922.

Chau, J. L., Urco, J. M., Avsarkisov, V., Vierinen, J. P., Latteck, R., Hall, C. M., & Tsutsumi, M. (2020). Four-Dimensional Quantification of Kelvin-Helmholtz Instabilities in the Polar Summer Mesosphere Using Volumetric Radar Imaging. *Geophysical Research Letters*, *47*(1), D09S12. doi: 10.1029/2019GL086081.

Dewan, E. M., & Picard, R. H. (1998, 3). Mesospheric bores. *Journal of Geophysical Research: Atmospheres*, *103*(D6), 6295–6305. Retrieved from `http://doi.wiley.com/10.1029/97JD02498` doi: 10.1029/97JD02498

Dewan, E. M., & Picard, R. H. (2001). On the origin of mesospheric bores. *Journal of Geophysical Research Atmospheres*. doi: 10.1029/2000JD900697.

Ecklund, W. L., & Balsley, B. B. (1981). Long-term observations of the Arctic mesosphere with the MST radar at Poker Flat, Alaska. *J. Geophys. Res.*, *86*(7775-7780). doi: 10.1029/JA086iA09p07775.

Feraco, F., Marino, R., Pumir, A., Primavera, L., Mininni, P. D., Pouquet, A., & Rosenberg, D. (2018). Vertical drafts and mixing in stratified turbulence: Sharp transition with Froude number. *EPL*, *123*(4), 44002. doi: 10.1209/0295-5075/123/44002.

Fritts, D. C., Baumgarten, G., Wan, K., Werne, J., & Lund, T. (2014). Quantifying Kelvin-Helmholtz instability dynamics observed in noctilucent clouds: 2. Modeling and interpretation of observations. *Journal of Geophysical Research:*

Atmospheres, *119*(15), 9359–9375. doi: 10.1002/2014JD021833.

Fritts, D. C., Kaifler, N., Kaifler, B., Geach, C., Kjellstrand, C. B., Williams, B. P., ... Wang, L. (2020). Mesospheric Bore Evolution and Instability Dynamics Observed in PMC Turbo Imaging and Rayleigh Lidar Profiling Over Northeastern Canada on 13 July 2018. *Journal of Geophysical Research: Atmospheres*. doi: 10.1029/2019JD032037.

Fritts, D. C., Williams, B. P., She, C. Y., Vance, J. D., Rapp, M., Lübken, F. J., ... Goldberg, R. A. (2004). Observations of extreme temperature and wind gradients near the summer mesopause during the MaCWAVE/MIDAS rocket campaign. *Geophysical Research Letters*. doi: 10.1029/2003GL019389.

Gardner, C. S., & Liu, A. Z. (2007). Seasonal variations of the vertical fluxes of heat and horizontal momentum in the mesopause region at Starfire Optical Range, New Mexico. *Journal of Geophysical Research Atmospheres*. doi: 10.1029/2005JD006179.

Gardner, C. S., Tao, X., & Papen, G. C. (1995). Simultaneous lidar observations of vertical wind, temperature, and density profiles in the upper mesophere: Evidence for nonseparability of atmospheric perturbation spectra. *Geophysical Research Letters*. doi: 10.1029/95GL02783.

Gudadze, N., Stober, G., & Chau, J. L. (2019). Can VHF radars at polar latitudes measure mean vertical winds in the presence of PMSE?. *Atmospheric Chemistry and Physics*, *19*(7), 4485–4497. doi: 10.5194/acp-19-4485-2019.

Hocking, W. K., Fuller, B., & Vandepeer, B. (2001, 1). Real-Time Determination of Meteor-Related Parameters Utilizing Modern Digital Technology. *Journal of Atmospheric and Solar-Terrestrial Physics*, *63*(2), 155–169.

Hoppe, U.-P., & Fritts, D. C. (1995). High-resolution measurements of vertical velocity with the European incoherent scatter VHF radar: 1. Motion field characteristics and measurement biases. *J. Geophys. Res.*, *100*(D8), 16813–16825. doi: 10.1029/95JD01466.

Hoppe, U.-P., Hall, C., & Röttger, J. (1988). First observations of summer polar mesospheric backscatter with a 224 MHz radar. *Geophysical Research Letters*, *15*(1), 28–31. doi: 10.1029/GL015i001p00028.

Hozumi, Y., Saito, A., Sakanoi, T., Yamazaki, A., Hosokawa, K., & Nakamura, T. (2019, 5). Geographical and Seasonal Variability of Mesospheric Bores Ob-

served from the International Space Station. *Journal of Geophysical Research: Space Physics*, *124*(5), 3775–3785. doi: 10.1029/2019JA026635

Hysell, D. L., & Chau, J. L. (2006). Optimal aperture synthesis radar imaging. *Radio Sci.*, *41*, RS2003. doi: 10.1029/2005RS003383.

Larsen, M. F., & Meriwether, J. W. (2012). Vertical winds in the thermosphere. *Journal of Geophysical Research: Space Physics*, *117*(9), A09319. doi: 10.1029/2012JA017843.

Latteck, R., Singer, W., Rapp, M., Vandepeer, B., Renkwitz, T., Zecha, M., & Stober, G. (2012). MAARSY: The new MST radar on Andøya – System description and first results. *Radio Sci.*, *47*(1), RS1006. doi: 10.1029/2011RS004775.

Lehmacher, G. A., Scott, T. D., Larsen, M. F., Bilén, S. G., Croskey, C. L., Mitchell, J. D., ... Collins, R. L. (2011). The Turbopause experiment: Atmospheric stability and turbulent structure spanning the turbopause altitude. *Annales Geophysicae*. doi: 10.5194/angeo-29-2327-2011.

Li, F., Swenson, G. R., Liu, A. Z., Taylor, M., & Zhao, Y. (2007). Investigation of a "wall" wave event. *Journal of Geophysical Research*, *112*(D4), D04104. doi: 10.1029/2006JD007213.

Lübken, F.-J., Jarvis, M. J., & Jones, G. O. L. (1999). First in situ temperature measurements at the Antarctic summer mesopause. *Geophysical Research Letters*, *26*(24), 3581–3584. doi: 10.1029/1999GL010719.

Marino, R., Rosenberg, D., Herbert, C., & Pouquet, A. (2015). Interplay of waves and eddies in rotating stratified turbulence and the link with kinetic-potential energy partition. *Europhysics Letters*, *112*(4). doi: 10.1209/0295-5075/112/49001.

Rapp, M., & Lübken, F.-J. (2004). Polar mesosphere summer echoes ({PMSE}): {Review} of observations and current understanding. *Atmospheric Chemistry and Physics*, *4*, 2601–2633. doi: 10.5194/acp-4-2601-2004.

Sato, K., Kohma, M., Tsutsumi, M., & Sato, T. (2017). Frequency spectra and vertical profiles of wind fluctuations in the summer Antarctic mesosphere revealed by MST radar observations. *Journal of Geophysical Research: Atmospheres*, *122*(1), 3–19. doi: 10.1002/2016JD025834.

Seyler, C. E. (2005, 5). Internal waves and undular bores in mesospheric inversion layers. *Journal of Geophysical Research: Atmospheres*, *110*(D9). doi: 10.1029/

2004JD004685

Smith, S. M., Stober, G., Jacobi, C., Chau, J. L., Gerding, M., Mlynczak, M. G., ... Umbriaco, G. (2017). Characterization of a Double Mesospheric Bore Over Europe. *Journal of Geophysical Research: Space Physics*, *122*(9), 9738–9750. doi: 10.1002/2017JA024225.

Smith, S. M., Taylor, M. J., Swenson, G. R., She, C. Y., Hocking, W., Baumgardner, J., & Mendillo, M. (2003). A multidiagnostic investigation of the mesospheric bore phenomenon. *Journal of Geophysical Research: Space Physics*, *108*(A2), 1–18. doi: 10.1029/2002JA009500

St.-Maurice, J.-P., & Chau, J. L. (2016). A theoretical framework for the changing spectral properties of meter-scale Farley-Buneman waves between 90 and 125 km altitudes. *Journal of Geophysical Research: Space Physics*, *121*(10), 310–341. doi: 10.1002/2016JA023105

Taylor, M. J., Turnbull, D. N., & Lowe, R. P. (1995). Spectrometric and imaging measurements of a spectacular gravity wave event observed during the ALOHA-93 Campaign. *Geophysical Research Letters*, *22*(20), 2849–2852. doi: 10.1029/95GL02948.

Thomas, G. E., & Olivero, J. J. (1986). The heights of polar mesospheric clouds. *Geophysical Research Letters*, *13*(13), 1403–1406. doi: 10.1029/GL013i013p01403.

Tippett, M. K., & Cohen, J. E. (2016). Tornado outbreak variability follows Taylor's power law of fluctuation scaling and increases dramatically with severity. *Nature Communications*, *7*, 10668. doi: 10.1038/ncomms10668.

Urco, J. M., Chau, J. L., Weber, T., & Latteck, R. (2019). Enhancing the spatio-temporal features of polar mesosphere summer echoes using coherent MIMO and radar imaging at MAARSY. *Atmospheric Measurement Techniques*, *12*, 955–969. doi: 10.5194/amt-12-955-2019.

Von Zahn, U., Lübken, F. J., & Putz, C. (1990). BUGATTI experiments: mass spectrometric studies of lower thermosphere eddy mixing and turbulence. *Journal of Geophysical Research*, *95*(D6), 7443–7465. doi: 10.1029/JD095iD06p07443.

Widdel, H.-U. (1991). Experimental evidence for solitary waves in the middle atmosphere. *Journal of Geophysical Research: Space Physics*, *96*(A9), 15931–15942. doi: 10.1029/91ja01396.

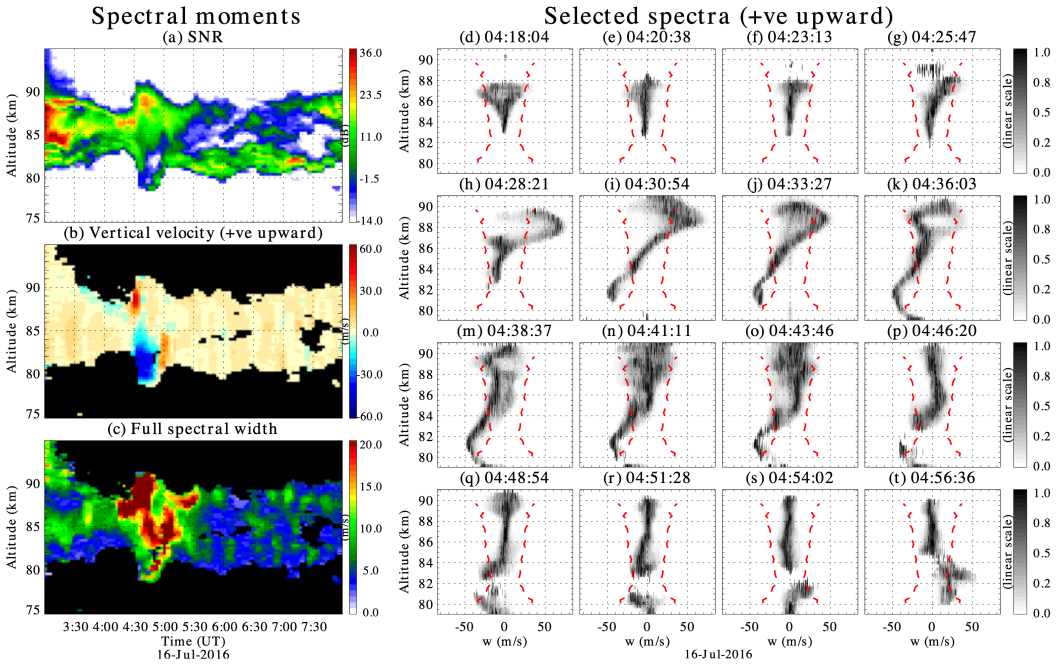

Figure 1. (Left) Range-time plots of: (a) signal-to-noise ratio (SNR), (b) vertical velocity (positive upward), and (c) total spectral width, observed with a vertical pointing beam on July 16, 2016. Note the relative large scales being shown for vertical velocities (± 60 ms^{-1}). (Right) Normalized spectra as a function of w, where $w = -f\lambda/2$, f is Doppler frequency in Hz, and λ the radar wavelength in meters. The normalization is in power spectra amplitude for each altitude with respect to its maximum. Three-sigma levels ($3\sigma_w$) based on June–July 2016 observations are plotted in dashed red lines.

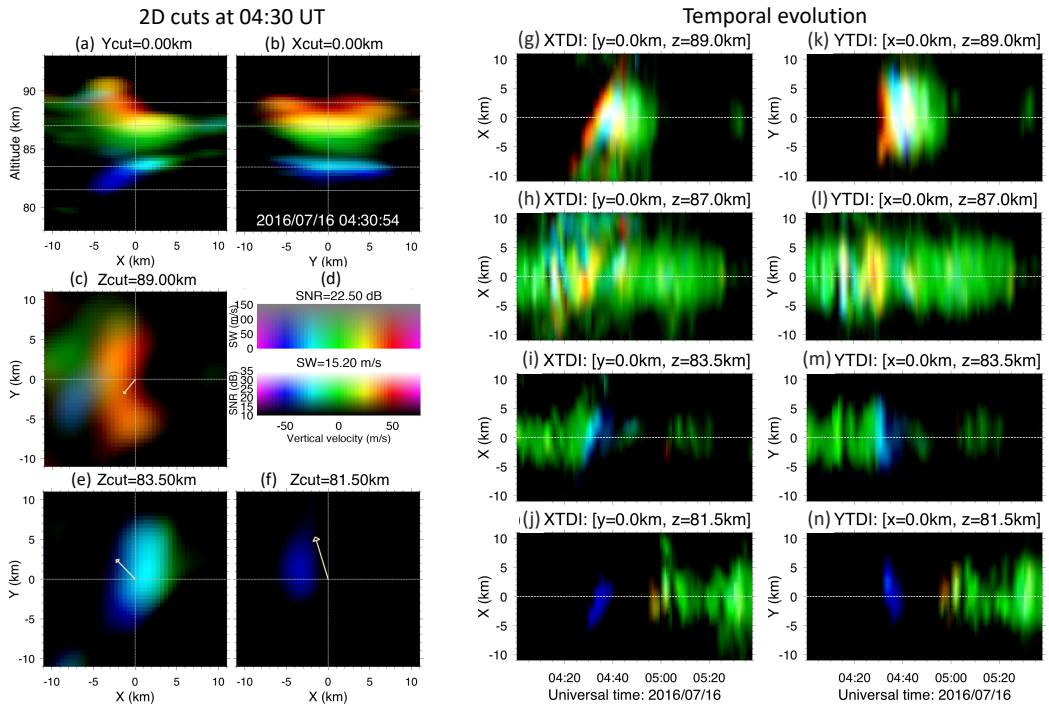

Figure 2. (Left) Two dimensional spatial cuts of PMSE inside the illuminated volume on July 16, 2016 around 0430 UT. xz and yz cuts at $x = 0$ and $y = 0$ km in panels (a) and (b), respectively. xy cuts at altitudes 89.0, 83.5, and 81.5 km in panels (c), (e), and (f), respectively. The intensity indicates signal strength of the echoes, while the color shows vertical velocity. Red (blue) values represent upward (downward) velocities greater (smaller) than 25 (-25) ms^{-1}, while green values represent velocities in between (see panel d). The 30-min horizontal wind from the specular meteor radar is indicated with a yellow arrow in the center of each xy cut. (Right) Space-time cuts at altitudes 89.0, 87.0, 83.5, and 81.5 km, of xy cuts in the left panel: (g-j) x versus time for $y = 0$, and (k-n) y versus time for $x = 0$.

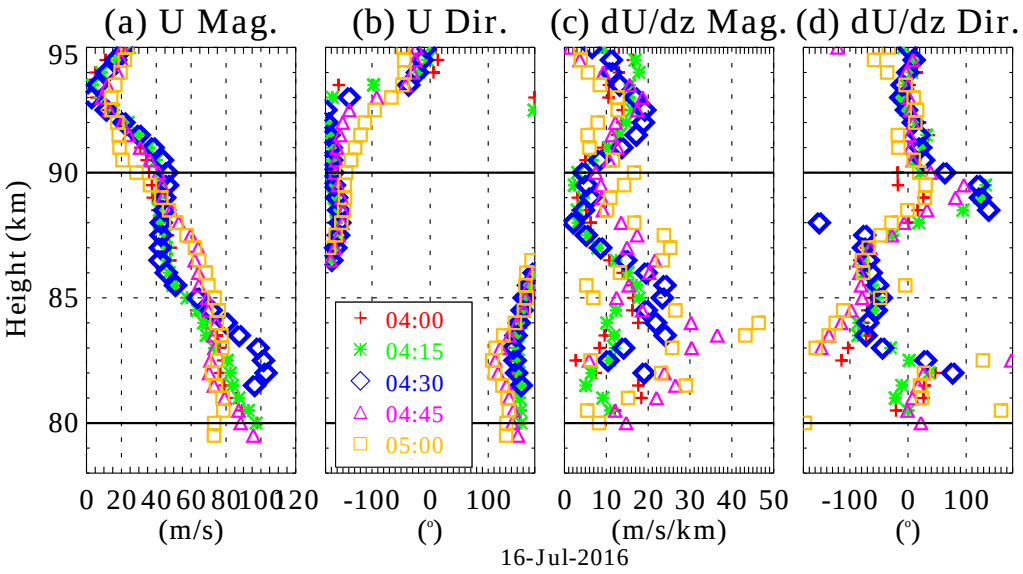

Figure 3. Horizontal winds profiles obtained with a collocated radar that observe specular meteor echoes around 04:30 UT on July 16, 2016: horizontal wind magnitude and direction with their respective vertical gradients. The direction is with respect to x, positive anti-clockwise. The colors indicate time in minutes with respect to 04:30 UT. The central time values are marked with black diamonds.

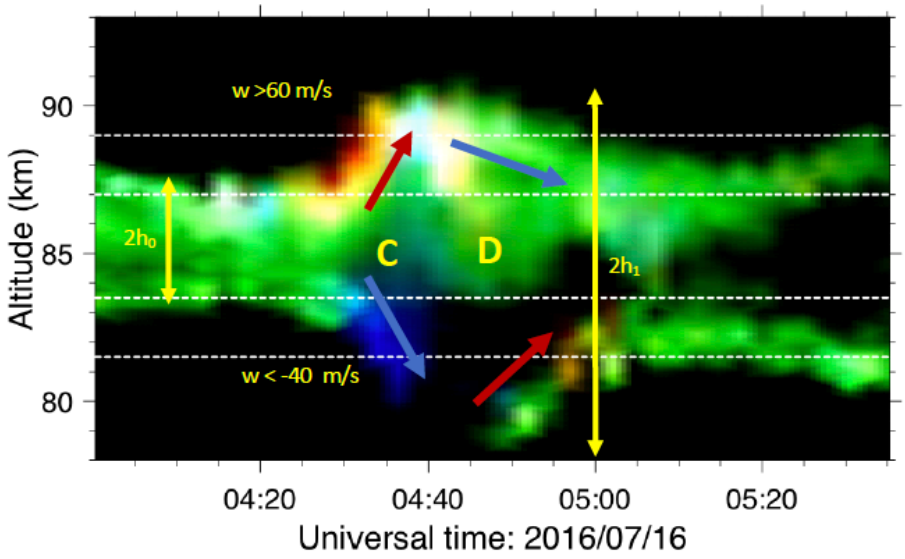

Figure 4. Closeup of the observations shown in Figure 1 to sketch the dynamics accompanying our event. The color code is the same as the one in Figure 2d. The regions of strong updraft (downdraft) are indicated with red (blue) arrows. Letter C and D represent horizontal wind convergence and divergence, respectively. Yellow vertical arrows indicate relevant vertical scales (see text).